On the Influence of Walking People on the Doppler Spectral Characteristics of Indoor Channels

Ahmed Abdelgawwad and Matthias Pätzold
Faculty of Engineering and Science, University of Agder
P.O. Box 509, 4898 Grimstad, Norway
Emails: {ahmed.abdel-gawwad, matthias.paetzold}@uia.no

***Abstract*—When modelling mobile radio channels with moving scatterers, it is generally assumed that the angles of departure (AODs), angles of arrival (AOAs), and the speed of the scatterers are time-invariant. However, this assumption is violated as the AODs and AOAs vary with the positions of the moving scatterers. Also, the speed of the moving scatterers might vary with time due to acceleration/deceleration. In this paper, we model the time-variant Doppler frequencies by taking into account the time-variant AODs, AOAs, and the variations of the speed of the moving scatterers. Furthermore, the complex channel gain of non-stationary single-input-single-output (SISO) fixed-to-fixed (F2F) indoor channels with moving and fixed scatterers is presented. The spectrogram of the complex channel gain using a Gaussian window is provided. The correctness of the analytical solutions is confirmed by simulations. The contribution of this paper paves the way towards the development of a passive in-home activity tracking system.**

I. Introduction

By 2060, around one third of the Europeans will be over 65 years old according to the report [1] released by the European Commission in 2015. At this point in time, the ratio between the working people and the retired seniors will become 2 to 1 instead of 4 to 1. The demand for in-home activity tracking of older people will increase to distinguish critical instances such as falls due to health problems from normal instances like walking, standing, and sitting down. This motivates us to analyze the Doppler spectral characteristics which is influenced by the in-home activity of older people.

In the literature, the Doppler effect caused by moving scatterers has been incorporated in wide-sense stationary vehicle-to-vehicle (V2V) [2], [3], fixed-to-fixed (F2F) [4], and fixed-to-mobile (F2M) [5] channel models. However, to the best of our knowledge, there is no study on the Doppler characteristics of non-stationary F2F indoor channels with moving people. In this paper, we apply the concept of the spectrogram to reveal the time-variant spectral information of non-stationary F2F indoor channels. The spectrogram is one of the time-frequency distributions that has many applications in music [6], [7], radar detection [8], earthquake records [9], and remote data sensing in underwater environments [10]. The concept of the spectrogram in the field of mobile radio channels has been first introduced in [11], where it has been applied to the estimation of the Doppler power spectral density of multipath fading channels. Later, it has been extended in [12] to reveal the time-variant spectral information of multipath fading channels by taking into account the speed variations of the mobile station. Moreover, the authors showed that the quality of the spectrogram can be improved by removing the spectral interference by averaging over the random channel phases of the multipath components. Other contributions to the reduction of the spectral interference can be found in, e.g., [13]–[15].

Our work starts with introducing a new indoor non-stationary SISO F2F channel model in which the locations of the scatterers are restricted to be inside a rectangular propagation area such as a room or an office. From this model, the time-variant AOAs, AODs, and their approximations using a first-order Taylor series are derived. Then, the time-variant Doppler frequencies based on the time-variant AOAs, AODs, and speeds are derived with their approximations using a first-order Taylor series. Based on these approximations, the instantaneous channel phases are presented. Using the instantaneous channel phases, the complex channel gain that consists of the sum of the plane wave components arriving from fixed and moving scatterers at the receiver is presented. The closed-form solution of the spectrogram of the complex channel gain is provided in this paper and represented as a sum of an auto-term and a cross-term. The auto-term of the spectrogram shows the desired time-variant spectral characteristics of each component of the complex channel gain. However, the cross-term, which represents the undesired spectral interference between the multipath components, affects the resolution of the spectrogram. In this paper, we use the method proposed in [12], [16] to reduce the effect of the cross-term. In addition, the time-variant mean Doppler shift and the time-variant Doppler spread will be derived using the spectrogram.

The rest of the paper is organized as follows. Section II presents the indoor F2F multipath propagation scenario. Section III derives the complex channel gain of the F2F

indoor non-stationary channel with time-variant AODs, AOAs, and speed of moving scatterers. Section IV shows the analytical solution of the spectrogram of the complex channel gain using a Gaussian window. Section V presents the numerical results and simulations. Section VI summarizes our contribution and discusses directions of future work.

II. The Indoor Multipath Propagation Scenario

The indoor multipath propagation scenario under consideration (see Fig. 1) consists of a room with length A and width B centralized at the origin O, a fixed transmitter (T_x) at position (x^T, y^T), and fixed receiver (R_x) at position (x^R, y^R). Also, the scenario includes N moving persons, which are modelled for simplicity by N moving point scatterers S_n^{M} $(n = 1, 2, \ldots, N)$ located at initial positions $(x_n^{\mathrm{M}}, y_n^{\mathrm{M}})$, where the trajectory of each scatterer is described by a time-variant speed $v_n(t)$ and a constant angle of motion (AOM) α_{v_n}. In addition, the scenario includes walls and fixed objects which are considered as sources for M fixed point scatterers S_m^{F} $(m = 1, 2, \ldots, M)$ located at positions $(x_m^{\mathrm{F}}, y_m^{\mathrm{F}})$. For simplicity, we model each moving (fixed) object as a single moving (fixed) scatterer. Single bounce scattering is assumed, i.e., each transmitted plane wave arrives at the receiver after a single bounce either on a fixed scatterer S_m^{F} or a moving scatterer S_n^{M}. Moreover, it is assumed that the T_x and R_x are equipped with single omnidirectional antennas. Furthermore, the line-of-sight (LOS) component is assumed to be obstructed. The initial Euclidean distance at time $t = 0$ between the moving scatterer S_n^{M} and T_x and between S_n^{M} and R_x are determined by

$$d_n^T = \sqrt{(x_n^{\mathrm{M}} - x^T)^2 + (y_n^{\mathrm{M}} - y^T)^2} \quad (1)$$

$$d_n^R = \sqrt{(x_n^{\mathrm{M}} - x^R)^2 + (y_n^{\mathrm{M}} - y^R)^2}, \quad (2)$$

respectively.

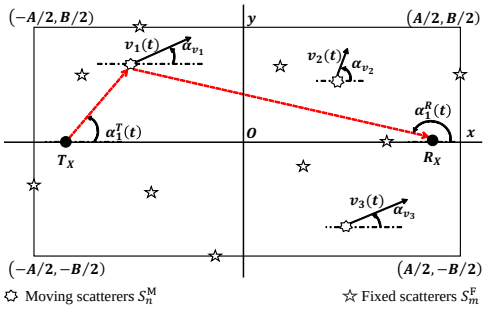

Fig. 1. An indoor propagation scenario with fixed scatterers S_m^{F} and moving scatterers S_n^{M}.

III. Derivation of The Complex Channel Gain

A. Modelling the Time-Variant Speed

The moving scatterers S_n^{M} in the considered multipath propagation scenario in the previous section have velocities $\vec{v}_n(t)$ for $n = 1, 2, \ldots, N$, which are expressed as vectors in Cartesian coordinates by $\vec{v}_n(t) = v_n(t)\cos(\alpha_{v_n})\,\hat{x} + v_n(t)\sin(\alpha_{v_n})\,\hat{y}$, where $\hat{x}$ ($\hat{y}$) denotes the x (y) direction. The time-variant speed of the nth moving scatterer S_n^{M} is given by

$$v_n(t) = v_n + a_n t \quad (3)$$

where v_n and a_n denote the initial speed of the nth moving scatterer and its acceleration/deceleration, respectively. From the speed of the moving scatterer, the time-variant positions $x_n(t)$ and $y_n(t)$ of the nth moving scatterer S_n^{M} can be calculated as follows

$$x_n^{\mathrm{M}}(t) = x_n^{\mathrm{M}} + \left[v_n t + \frac{1}{2}a_n t^2\right]\cos(\alpha_{v_n}) \quad (4)$$

$$y_n^{\mathrm{M}}(t) = y_n^{\mathrm{M}} + \left[v_n t + \frac{1}{2}a_n t^2\right]\sin(\alpha_{v_n}), \quad (5)$$

respectively. The parameters x_n^{M} and y_n^{M} are the initial x and y coordinates of the nth moving scatterer S_n^{M}, respectively.

B. Modelling the Time-Variant AODs and AOAs

The time-variant AOD $\alpha_n^T(t)$ is defined as the angle between the direction of the transmitted wave travelling towards the nth moving scatterer S_n^{M} and the positive x-axis. According to Fig.1, $\alpha_n^T(t)$ can be expressed as

$$\alpha_n^T(t) = \arctan\left(\frac{y_n^{\mathrm{M}}(t) - y^T}{x_n^{\mathrm{M}}(t) - x^T}\right). \quad (6)$$

Similarly, the time-variant AOA $\alpha_n^R(t)$ is determined by the angle between the direction of the wave travelling from the nth moving scatterer S_n^{M} to R_x and the positive x-axis. The AOA $\alpha_n^R(t)$ can be expressed as

$$\alpha_n^R(t) = \arctan\left(\frac{y_n^{\mathrm{M}}(t) - y^R}{x_n^{\mathrm{M}}(t) - x^R}\right). \quad (7)$$

From (6) and (7), the AODs $\alpha_n^T(t)$ and AOAs $\alpha_n^R(t)$ are non-linear functions of time t. However, using the first-order Taylor series, they can be approximated by the following expressions

$$\alpha_n^T(t) \approx \alpha_n^T + \gamma_n^T t \quad (8)$$

$$\alpha_n^R(t) \approx \alpha_n^R + \gamma_n^R t \quad (9)$$

where

$$\alpha_n^T = \alpha_n^T(t)|_{t=0} = \arctan\left(\frac{y_n^{\mathrm{M}} - y^T}{x_n^{\mathrm{M}} - x^T}\right) \quad (10)$$

$$\alpha_n^R = \alpha_n^R(t)|_{t=0} = \arctan\left(\frac{y_n^{\mathrm{M}} - y^R}{x_n^{\mathrm{M}} - x^R}\right) \quad (11)$$

$$\gamma_n^T = \frac{d}{dt}\alpha_n^T(t)|_{t=0} = \frac{v_n \sin\left(\alpha_{v_n} - \alpha_n^T\right)}{d_n^T} \quad (12)$$

$$\gamma_n^R = \frac{d}{dt}\alpha_n^R(t)|_{t=0} = \frac{v_n \sin\left(\alpha_{v_n} - \alpha_n^R\right)}{d_n^R}. \quad (13)$$

C. Modelling the Time-Variant Doppler Frequencies

Due to the Doppler effect, the instantaneous time-variant Doppler frequency introduced by the nth moving scatterer with time-variant speed $v_n(t)$, AOA $\alpha_n^R(t)$, and AOD $\alpha_n^T(t)$ is given by [2], [5]

$$\begin{aligned} f_n(t) &= -f_{n,\max}(t)[\cos\left(\alpha_n^T(t) - \alpha_{v_n}\right) \\ &+ \cos\left(\alpha_{v_n} - \alpha_n^R(t)\right)] \end{aligned} \quad (14)$$

where

$$f_{n,\max}(t) = \frac{f_0 v_n(t)}{c_0} \quad (15)$$

denotes the maximum time-variant Doppler frequency due to the speed of the nth moving scatterer.

The parameters f_0 and c_0 in (15) represent the carrier frequency and the speed of light, respectively. The expression of the Doppler frequency introduced by the nth moving scatterer S_n^{M} in (14) can be simplified using the first-order Taylor series. This simplified expression is given by

$$f_n(t) \approx f_n + k_n t \quad (16)$$

where

$$\begin{aligned} f_n &= f_n(0) \\ &= -f_{n,\max}\left[\cos\left(\alpha_n^T - \alpha_{v_n}\right) + \cos\left(\alpha_{v_n} - \alpha_n^R\right)\right] \quad (17) \\ k_n &= \frac{d}{dt} f_n(t)|_{t=0} \\ &= f_{n,\max}\Bigg\{\gamma_n^T \sin\left(\alpha_n^T - \alpha_{v_n}\right) - \gamma_n^R \sin\left(\alpha_{v_n} - \alpha_n^R\right) \\ &\quad - \frac{a_n}{v_n}\left[\cos\left(\alpha_n^T - \alpha_{v_n}\right) + \cos\left(\alpha_{v_n} - \alpha_n^R\right)\right]\Bigg\} \quad (18) \end{aligned}$$

in which $f_{n,\max}$ is the initial maximum Doppler frequency at $t = 0$, i.e, $f_{n,\max} = f_{n,\max}(0) = f_0 v_n / c_0$. The term k_n in (18) can be expressed as the sum of four terms. The first and second terms are due to the rate of change of the AOD and AOA respectively, and the third and fourth terms correspond to the acceleration (deceleration) of the nth moving scatterer. For the given indoor propagation scenario, if the parameters given by (10)–(13) and α_{v_n} are constant, the time-variant Doppler frequency $f_n(t)$ is a deterministic process. Otherwise, $f_n(t)$ becomes a stochastic process if at least one of these parameters or more are random variables. It should be mentioned that, if we set the parameters γ_n^R, γ_n^T, and a_n to zero, the expressions in (14) and (16) reduce to $f_n = -f_{n,\max}\left[\cos\left(\alpha_n^T - \alpha_{v_n}\right) + \cos\left(\alpha_{v_n} - \alpha_n^R\right)\right]$, which represents the Doppler shift caused by a moving scatterer S_n^{M} in stationary channels without velocity variations [2]–[5].

D. Time-Variant Channel Phases and Complex Channel Gain

The time-variant channel phases using the instantaneous Doppler frequency in (16) are calculated according to [17] as

$$\theta_n(t) = 2\pi \int_{-\infty}^{t} f_n(x)dx \approx \theta_n + 2\pi\left(f_n t + \frac{k_n}{2} t^2\right) \quad (19)$$

where the first term θ_n is the initial channel phase, which can be modelled as a random variable with uniform distribution over the interval between 0 and 2π (i.e., $\mathcal{U} \sim (0, 2\pi)$) [17]. After the instantaneous channel phase is obtained, we can express the complex channel gain consisting of $N + M$ paths in non-line-of-sight environments as

$$\mu(t) = \sum_{n=1}^{N} c_n e^{j\left[2\pi\left(f_n t + \frac{k_n}{2} t^2\right) + \theta_n\right]} + \sum_{m=1}^{M} c_m e^{j\theta_m}. \quad (20)$$

The first term in (20) represents the sum of multipath components coming from N moving scatterers. It has to be mentioned that, this term is analogous to the complex channel gain of the models presented in [12], [16], [17]. The second term denotes the sum of multipath components coming from M fixed scatterers. The parameter c_n (c_m) represents the attenuation that happens due to the interaction between the signal and the nth moving (mth fixed) scatterer. The phase shift θ_n (θ_m) is caused by the signal interaction with the na moving scatterer S_n^{M} for $n = 1, 2, \ldots, N$ (mth fixed scatterer S_n^{F} for $m = 1, 2, \ldots, M$) scatterer. These quantities are supposed to be identically and independently distributed (i.i.d.) random variables each with uniform distribution between 0 and 2π. The model expressed by (20) is a non-stationary indoor channel model. From this model, the time-variant mean Doppler shift and Doppler spread can be expressed according to [17] as

$$B_f^{(1)}(t) = \frac{\sum_{n=1}^{N} c_n^2 f_n(t)}{\sum_{n=1}^{N} c_n^2 + \sum_{m=1}^{M} c_m^2} \quad (21)$$

and

$$B_f^{(2)}(t) = \sqrt{\frac{\sum_{n=1}^{N} c_n^2 f_n^2(t)}{\sum_{n=1}^{N} c_n^2 + \sum_{m=1}^{M} c_m^2} - \left(B_f^{(1)}(t)\right)^2}, \quad (22)$$

respectively. In the next section, the spectrogram analysis will be presented in order to identify the spectral behaviour of the proposed model.

IV. Spectrogram Analysis Using a Gaussian Window

The main idea behind the spectrogram is to divide the time-variant signal into short-time overlapping signals. This is done by multiplying this signal with a short-time signal (sliding window) $h(t)$. Then, the Fourier-transform of each overlapping signal is calculated to get the so-called short-time Fourier transform (STFT). Finally, the STFT is multiplied by its complex conjugate to obtain the spectrogram. This concept is used to identify the spectral behavior of time-variant deterministic or stochastic signals. The Gaussian window function is defined as

$$h(t) = \frac{1}{\sqrt{\sigma_w}\pi^{1/4}} \; e^{-\frac{t^2}{2\sigma_w^2}} \quad (23)$$

where σ_w is called the window spread. A high value of the window spread σ_w results in a high frequency resolution and a low time localization and vice versa. Hence, choosing the window size is always a trade-off between the time and frequency resolutions. The window used to calculate the spectrogram is real, positive, and even. It has also a unit energy (i.e., $\int_{-\infty}^{\infty} h^2(t)dt = 1$). After multiplying the complex channel gain presented in (20) by the window function in (23), we can express the short-time complex channel gain as follows

$$x(t', t) = \mu(t')h(t' - t) \tag{24}$$

where t denotes the local time in which we want to analyze the spectral properties of the complex channel gain, and t' is the running time. The window is centralized around the local time t in (24). The STFT of the complex channel gain $\mu(t)$ is obtained by computing the Fourier transform of (24) w.r.t. the running time t', i.e.,

$$X(f, t) = \int_{-\infty}^{\infty} x(t', t)e^{-j2\pi ft'}dt'. \tag{25}$$

Finally, the spectrogram of the complex channel gain $\mu(t)$ in (20) is obtained by multiplying (25) by its complex conjugate. It can be represented as

$$S_\mu(f, t) = |X(f, t)|^2. \tag{26}$$

After substituting the complex channel gain presented in (20) and the Gaussian window function according to (23) in (24) and applying the Fourier transformation with respect to t' [see (25)], we obtain the following closed-form solution of the STFT of the complex channel gain

$$X(f,t) = \frac{e^{-j2\pi ft}}{\sqrt{\sigma_w}\pi^{1/4}}\Bigg[\sum_{n=1}^{N}\mu_n(t)\,G(f, f_n(t), \sigma_{x,n}^2) + \sum_{m=1}^{M}\mu_m(t)G(f, 0, \sigma_{x,m}^2)\Bigg] \tag{27}$$

where

$$G(f, f_n(t), \sigma_x^2) = \frac{e^{-\frac{(f-f_n(t))^2}{2\sigma_x^2}}}{\sqrt{2\pi}\sigma_x} \tag{28}$$

$$\sigma_{x,n}^2 = \frac{1 - j2\pi\sigma_w^2 k_n}{(2\pi\sigma_w)^2} \tag{29}$$

$$\sigma_{x,m}^2 = \frac{1}{(2\pi\sigma_w)^2}. \tag{30}$$

In the equations above, the function $f_n(t)$ and the parameter k_n are given by (16) and (18), respectively. After substituting (27) in (26), we get the spectrogram of the complex channel gain $\mu(t)$. By using the results in [16], the spectrogram $S_\mu(f, t)$ in (26) can be expressed in closed form as

$$S_\mu(f, t) = S_\mu^{(a)}(f, t) + S_\mu^{(c)}(f, t) \tag{31}$$

where $S_\mu^{(a)}(f, t)$ is called the *auto-term*, and the second term $S_\mu^{(c)}(f, t)$ denotes the *cross-term*. The auto-term is given by

$$S_\mu^{(a)}(f, t) = \sum_{n=1}^{N} c_n^2 G(f, f_n(t), \sigma_n^2) + \sum_{m=1}^{M} c_m^2 G(f, 0, \sigma_m^2) \tag{32}$$

where

$$\sigma_n^2 = \frac{1 + (2\pi\sigma_w^2 k_n)^2}{2(2\pi\sigma_w)^2} \tag{33}$$

$$\sigma_m^2 = \frac{1}{2(2\pi\sigma_w)^2}. \tag{34}$$

The auto-term $S_\mu^{(a)}(f, t)$ in (32) is a real and positive function that represents the desired spectral characteristics of the channel due to the time-variant Doppler frequencies. The result in (32) states that $S_\mu^{(a)}(f, t)$ can be expressed as a sum of Gaussian functions weighted by the squared path gains c_n^2 and c_m^2 for moving and fixed scatterers, respectively, and centralized at their corresponding instantaneous Doppler frequencies. The weighted Gaussian functions of the first term of the auto-term $S_\mu^{(a)}(f, t)$ in (32) are centralized at the instantaneous Doppler frequencies introduced by the moving scatterers. In the second term of (32), the weighted Gaussian functions are centralized at zero frequency, as stationary scatterers do not cause Doppler shifts in F2F channels. An interesting observation is that the variance σ_n^2 in (34) of the Gaussian function $G(f, f_n(t), \sigma_n^2)$ of the first term of the auto-term $S_\mu^{(a)}(f, t)$ depends on the parameter k_n, which determines the rate of change of the Doppler frequency in (16).

The cross-term $S_\mu^{(c)}(f, t)$ of the spectrogram is presented in (35), where $\mu_n(t)$ and $\mu_m(t)$ are the complex gains corresponding to the moving scatterer S_n^{M} and the fixed scatterer S_n^{F}, respectively is considered as the undesired spectral interference component. This term consists of a sum of $(N + M)(N + M - 1)/2$ components. From (35), it is obvious that the cross-term is real valued, but not necessarily positive. In order to remove the cross-term, the statistical average over the random channel phases θ_n of the spectrogram has to be taken [12], i.e,

$$E\left\{S_\mu(f, t)\right\}\Big|_{\theta_n} = E\left\{S_\mu^{(a)}(f, t)\right\}\Big|_{\theta_n} + E\left\{S_\mu^{(c)}(f, t)\right\}\Big|_{\theta_n} = S_\mu^{(a)}(f, t) \tag{36}$$

where $E\{\cdot\}$ is the expectation operator. The reason behind canceling the cross-term $S_\mu^{(c)}(f, t)$ by taking the average over θ_n is that $E\{e^{j(\theta_n - \theta_m)}\}$ equals zero in the case of $n \neq m$. Note that the auto-term $S_\mu^{(a)}(f, t)$ is not affected by taking the average over θ_n, as $E\{e^{j(\theta_n - \theta_m)}\} = 1$ for $n = m$. This method requires many sample functions of $S_\mu(f, t)$, which can be generated for different realizations of θ_n and θ_m. Then, the spectrograms of each trial will be

$$S_{\mu}^{(c)}(f,t)=\frac{2}{\sigma_w\sqrt{\pi}}\Bigg[\sum_{n=1}^{N-1}\sum_{m=n+1}^{N}\Re\Big\{G(f,f_n(t),\sigma_{x,n}^2)\,G^*(f,f_m(t),\sigma_{x,m}^2)\,\mu_n(t)\,\mu_m^*(t)\Big\}+\sum_{m=1}^{M-1}\sum_{n=m+1}^{M}\Re\Big\{$$
$$G(f,0,\sigma_{x,m}^2)G^*(f,0,\sigma_{x,n}^2)\,\mu_m(t)\,\mu_n^*(t)\Big\}+\sum_{n=1}^{N}\sum_{m=1}^{M}\Re\Big\{G(f,f_n(t),\sigma_{x,n}^2)\,G^*(f,0,\sigma_{x,m}^2)\,\mu_n(t)\,\mu_m^*(t)\Big\}\Bigg] \tag{35}$$

summed up and divided by the total number of trials, and hence, the cross-term approaches zero. The results of this method will be presented in Section V.

Since the auto-term $S_{\mu}^{(a)}(f,t)$ in (32) contains the desired spectral information of the channel, one can calculate the time-variant mean Doppler shift $B_{\mu}^{(1)}(t)$ as follows

$$B_{\mu}^{(1)}(t)=\frac{\int_{-\infty}^{\infty}fS_{\mu}^{(a)}(f,t)}{\int_{-\infty}^{\infty}S_{\mu}^{(a)}(f,t)}. \tag{37}$$

Analogously, the time-variant Doppler spread $B_{\mu}^{(2)}(t)$ can be obtained from the auto-term $S_{\mu}^{(a)}(f,t)$ and is given by means of

$$B_{\mu}^{(2)}(t)=\sqrt{\frac{\int_{-\infty}^{\infty}f^2S_{\mu}^{(a)}(f,t)}{\int_{-\infty}^{\infty}S_{\mu}^{(a)}(f,t)}-\Big(B_{\mu}^{(1)}(t)\Big)^2}. \tag{38}$$

V. Numerical Results and Simulations

In this section, simulations and numerical results are presented for an indoor scenario with certain parameters. The value for the carrier frequency f_0 has been set to 5.9 GHz. The spectral behavior of the channel was studied over the interval from $t=0$ to 5 s. With reference to Fig. 2, the chosen values for the length A and the width B of the room were 10 m and 5 m, respectively. The locations of T_x and R_x were $(-3.5,\,2.4)$ and $(-4.9,\,0)$, respectively. The number of the moving scatterers (persons) N was chosen to be 3, and the number of fixed scatterers (walls and other objects) M was equal to 7.

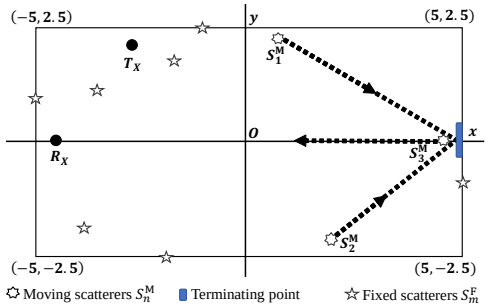

Fig. 2. The chosen scenario illustrates the locations of T_x, R_x, and the moving scatterers as well as their directions of motion.

In the considered scenario, the first two moving scatterers S_1^{M} and S_2^{M}, which start from different locations, and move towards the same destination (termination) point at constant initial speeds. Then, they start to decelerate until they reach the termination point with zero speed value and stop moving. The third scatterer S_3^{M} moves away from the termination point along a horizontal line at a constant speed and during the whole observation interval. The motion directions of the moving scatterers are indicated in Fig. 2 by dashed lines. In order to simulate this scenario, the initial locations of the moving scatterers S_1^{M}, S_2^{M}, and S_3^{M} according to Fig. 2 are $(1,\,2)$, $(-2,\,2)$, and $(4.5,\,0)$, respectively, and the termination point of S_1^{M} and S_2^{M} is located at $(5,\,0)$. The AOMs of S_1^{M} and S_2^{M} are computed based on their initial locations and the termination point. The AOM of the moving scatterer S_3^{M} is π rad. The initial speed of each of the moving scatterers is 1 m/s and the deceleration parameters of S_1^{M} and S_2^{M} are $-0.5\,\mathrm{m/s^2}$. The path gains of the moving and fixed scatterers were calculated from the following equations

$$c_n=\sigma_0\sqrt{\frac{2\eta_N}{N}}\qquad\text{and}\qquad c_m=\sigma_0\sqrt{\frac{2\eta_M}{M}} \tag{39}$$

respectively. The parameters η_N and η_M were used to determine the contribution of the moving and fixed scatterers, such that $\eta_N+\eta_M=1$. The chosen values of σ_0, η_N and η_M are 1, 0.5, and 0.5, respectively. The time-variant Doppler frequencies introduced by the moving scatterers are shown in Fig. 3. This figure depicts the Doppler frequencies of the moving scatterers after substituting the exact expression of the AODs and AOAs given by (6) and (7), respectively in (14). Also, Fig. 3 depicts the approximate solution of the time-variant Doppler frequencies according to (16). Since, the moving scatterers S_1^{M} and S_2^{M} have three speed states, their approximated time-variant Doppler frequencies using Taylor series have three states, which can be expressed as follows

$$f_n(t)=\begin{cases}f_{n,1}+k_{n,1}t, & \text{if } 0\le t<t_{n,1},\\ f_{n,2}+k_{n,2}(t-t_{n,1}), & \text{if } t_{n,1}\le t<t_{n,2},\\ f_{n,3}, & \text{if } t_{n,2}\le t\end{cases}$$

for $n=1,2$. The time instants $t_{n,1}$ and $t_{n,2}$ are those in which the moving scatterers start to decelerate and stop moving, respectively. The parameter $k_{n,2}$ is evaluated at the time instance $t_{n,2}$, which means that γ_n^T, γ_n^R, α_n^T, and α_n^R were evaluated at the same time instant. It is shown in Fig. 3 that the approximations represented in (16) deviate from the exact solution according to (14). These deviations happen due to the approximation of the AODs and AOAs given by (8) and (9), respectively. The analysis and simulations of the spectrogram are shown in Figs. 4 and 5, respectively.

We have chosen $\sigma_w = 1/\sqrt{2\pi|k_{1,2}|}$ [16]. The figures show that the results of the analytical solution in (31) are similar to those of the simulations. They also show how the cross-term of the spectrogram interferes with the auto-term. This happens especially with the spectrum of the fixed scatterers at $f = 0\,\text{Hz}$, as they are about to vanish. The effect of the cross-term is also obvious starting from time $t \approx 4\,\text{s}$. It should be mentioned that the parameters θ_n and θ_m are the same for the analysis and the simulation. Figure 4 shows the auto-term of the spectrogram according to (32). In Fig. 6, the simulations of the spectrogram are depicted, after taking the average over multiple trials as mentioned in Section IV. The simulations in Fig. 6 show a perfect removal of the cross-term such that the spectrogram approaches the auto-term depicted in Fig. 7. After removing the cross-term, the spectral lines become clearer, especially those of the fixed scatterers at $f = 0\,\text{Hz}$ and after $t \approx 4\,\text{s}$.

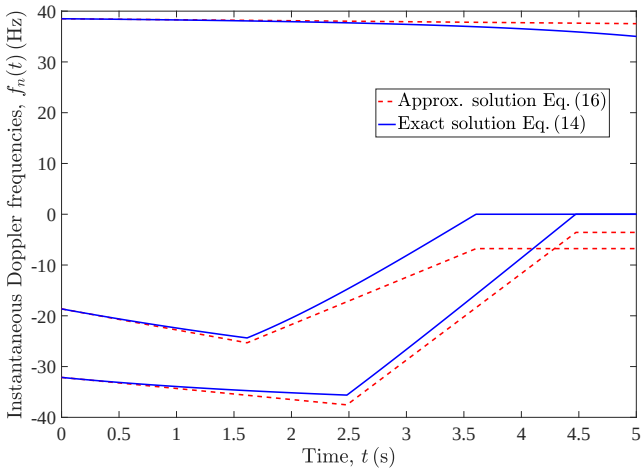

Fig. 3. Instantaneous Doppler frequencies caused by the moving scatterers using the exact expression in (14) and the approximation in (16).

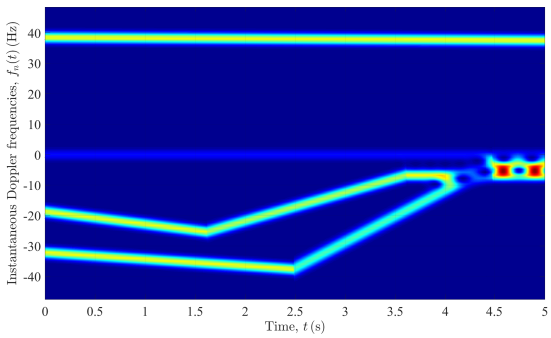

Fig. 4. Spectrogram $S_\mu(f,t)$ of the complex channel gain $\mu(t)$ according to (31).

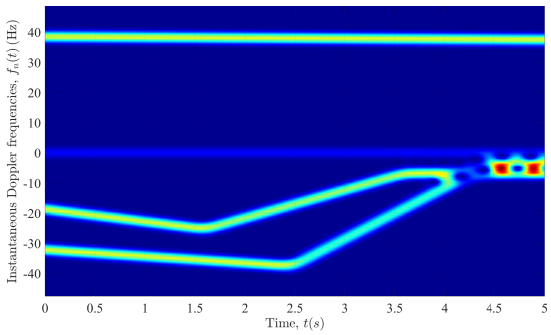

Fig. 5. Spectrogram $S_\mu(f,t)$ (simulation) of the complex channel gain $\mu(t)$.

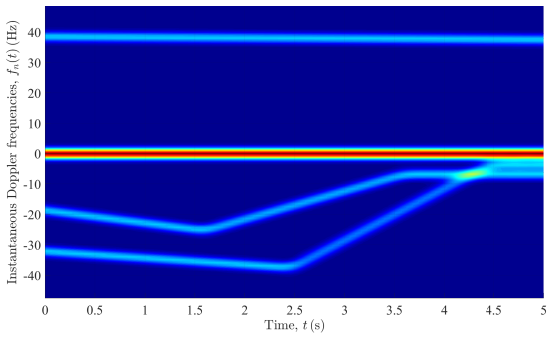

Fig. 6. Spectrogram $S_\mu(f,t)$ (simulation) of the complex channel gain $\mu(t)$ after taking the average over the channel phases θ_n.

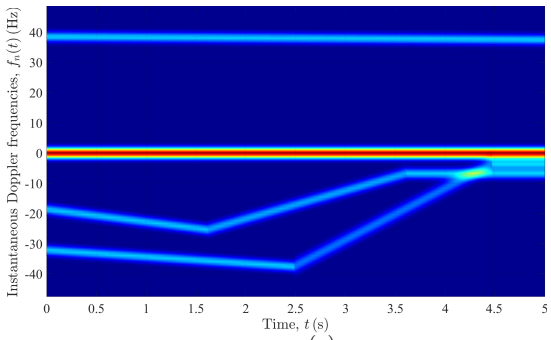

Fig. 7. Auto-term of the spectrogram $S_\mu^{(a)}(f,t)$ of the complex channel gain $\mu(t)$ according to (32).

Fig. 8 depicts the time-variant mean Doppler shift $B_f^{(1)}(t)$ after substituting (14) and (16) in (21). This figure shows the deviations between the time-variant mean Doppler shift after substituting the exact expression given by (14) and the approximation expressed by (16) in (21). These deviations occur due to the approximation using the Taylor series of the AODs and AOAs given by (8) and (9), respectively. Also, Fig. 8 depicts the time-variant mean Doppler shift $B_\mu^{(1)}(t)$ after applying (37) to the auto-term given by (32) and to the simulation of the spectrogram after taking the average over the random phases. This figure shows a perfect match between $B_f^{(1)}(t)$ and $B_\mu^{(1)}(t)$, meaning that the proposed channel model is consistent w.r.t the time-variant mean Doppler shift [17].

Fig. 9 depicts the time-variant Doppler spread $B_f^{(2)}(t)$. This figure shows the deviations between the time-variant Doppler spread after substituting the exact expression given by (14) and the approximation expressed by (16) in (22). Also, Fig. 9 depicts the time-variant Doppler spread $B_\mu^{(2)}(t)$ after applying (38) to the auto-term given by (32) and to the simulation of the spectrogram after taking the average over the random phases. This figure shows a perfect match between $B_f^{(2)}(t)$ and $B_\mu^{(2)}(t)$, i.e, the model is also consistent w.r.t the time-variant Doppler spread [17].

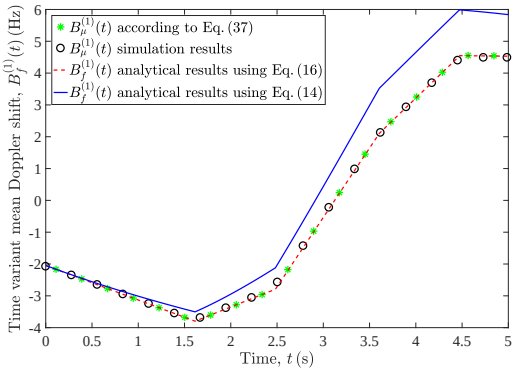

Fig. 8. Time-variant mean Doppler shifts $B_f^{(1)}(t)$ and $B_\mu^{(1)}(t)$ obtained from (21) and (37), respectively.

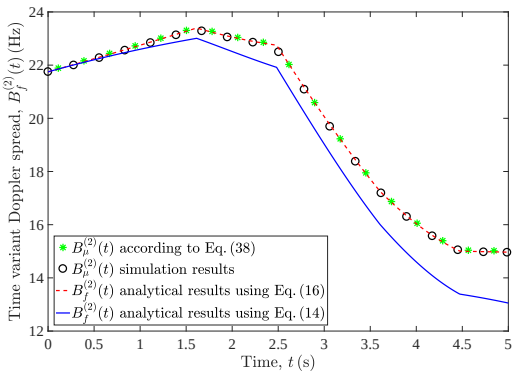

Fig. 9. Time-variant Doppler spreads $B_f^{(2)}(t)$ and $B_\mu^{(2)}(t)$ computed according to (22) and (38), respectively.

VI. Conclusion

In this paper, we presented the spectrogram of indoor non-stationary F2F channels with fixed and moving scatterers. We derived the time-variant channel parameters, their approximations, and the complex channel gain from the geometrical model. Then, a closed-form solution of the spectrogram using a Gaussian window was presented. Moreover, we introduced how the cross-term of the spectrogram can be eliminated by taking the average over the random channel phases. Furthermore, we showed how to calculate the time-variant mean Doppler shift and Doppler spread from the spectrogram. Finally, a good match between the results of the analysis and the simulations was shown. This model is beneficial for passive fall detection systems because it reveals the time-variant spectral information in the case of walking scenarios. For future work, we propose to extend this model to three-dimensional (3D) MIMO channels as the MIMO techniques allow to reduce the cross-term of the spectrogram by taking the average in the spatial domain rather than taking the average over the random phases. Also, we propose to extend this model to 3D geometry so that the spectral information can be analyzed in the case of 3D motions such as, standing, sitting, falling or jumping.

References

[1] The European Commission, "The 2015 ageing report: underlying assumptions and projection methodologies," *European Economy*, August 2014, DOI: 10.2765/76255.

[2] A. Borhani and M. Pätzold, "Modeling of vehicle-to-vehicle channels in the presence of moving scatterers," in *Proc. IEEE 76th Vehicular Technology Conference, VTC2012-Fall*. Quebec City, Canada, Sep. 2012.

[3] A. Zajić, "Modeling impact of moving scatterers on Doppler spectrum in wideband vehicle-to-vehicle channels," in *2015 9th European Conference on Antennas and Propagation (EuCAP)*, May 2015, pp. 1–5.

[4] X. Zhao, Q. Han, X. Liang, B. Li, J. Dou, and W. Hong, "Doppler spectra for F2F radio channels with moving scatterers," *IEEE Transactions on Antennas and Propagation*, vol. 64, no. 9, pp. 4107–4112, Sept 2016.

[5] V. H. Pham, M. H. Taieb, J. Y. Chouinard, S. Roy, and H. T. Huynh, "On the double Doppler effect generated by scatterer motion," *REV Journal on Electronics and Communications*, vol. 1, no. 1, pp. 30–37, Mar. 2011.

[6] J. F. Alm and J. S. Walker, "Time-frequency analysis of musical instruments," *SIAM Review*, vol. 44, no. 3, pp. 457–476, 2002.

[7] S. K. Banchhor and A. Khan, "Musical instrument recognition using spectrogram and autocorrelation," *Int. J. Soft Computing and Engineering*, vol. 2, no. 1, pp. 1–4, Mar. 2012.

[8] R. I. A. Harmanny, J. J. M. de Wit, and G. Prémel Cabic, "Radar micro-Doppler feature extraction using the spectrogram and the cepstrogram," in *Proc. 11th European Radar Conference, EuRAD 2014*, Oct. 2014, pp. 165–168.

[9] C. I. Huerta-Lopez, Y. J. Shin, E. J. Powers, and J. M. Roesset, "Time-frequency analysis of earthquake records," in *Proc. 12th World Conf. on Earthquake Engineering, 12WCEE2000*, vol. 33. Auckland, New Zealand, Feb. 2000, pp. 1–9.

[10] T. A. Lampert and S. E. M. O'Keefe, "A survey of spectrogram track detection algorithms," *Applied Acoustics*, vol. 71, no. 2, pp. 87–100, Feb. 2010.

[11] M. Pätzold and N. Youssef, "Spectrogram analysis of multipath fading channels," in *Proc. 26th IEEE Personal, Indoor and Mobile Radio Communications, PIMRC 2015*. Hong Kong, China, Aug./Sep. 2015.

[12] M. Pätzold and C. A. Gutiérrez, "Spectrogram analysis of multipath fading channels under variations of the mobile speed," in *Proc. 84rd IEEE Veh. Technol. Conf., IEEE VTC2016-Fall*. Montreal, Canada, Sep. 2016.

[13] D. Gabor, "Theory of communication," *J. IEE*, vol. 93[III], pp. 429–457, Nov. 1946.

[14] A. W. Rihaczek, "Signal energy distribution in time and frequency," *IEEE Trans. Inform. Theory*, vol. 14, no. 3, pp. 369–374, May 1968.

[15] L. Cohen, "Time-frequency distributions–A review," *Proceedings of the IEEE*, vol. 77, no. 7, pp. 941–981, Jul. 1989.

[16] M. Pätzold, C. A. Gutiérrez, and N. Youssef, "Enhancing the resolution of the spectrogram of non-stationary channels by using massive MIMO techniques," in *Proc. IEEE 86th Vehicular Technology Conference, VTC2017-Fall*. Toronto, Canada, 2017.

[17] ——, "On the consistency of non-stationary multipath fading channels with respect to the average Doppler shift and the Doppler spread," in *Proc. IEEE Wireless Communications and Networking Conference, WCNC 2017*. San Francisco, CA, USA, Mar. 2017.